J. Fluid Mech. (2000), *vol.* 406, *pp.* 1–26. Printed in the United Kingdom

Nonlinear equilibrium solutions for the channel flow of fluid with temperature-dependent viscosity

By D. P. WALL† AND M. NAGATA‡

School of Mathematics and Statistics, University of Birmingham, Edgbaston, Birmingham B15 2TT, UK

(Received 23 September 1998 and in revised form 13 July 1999)

The nonlinear stability of the channel flow of fluid with temperature-dependent viscosity is considered for the case of vanishing Péclet number for two viscosity models, $\mu(T)$, which vary monotonically with temperature, T. In each case the basic state is found to lose stability from the linear critical point in a subcritical Hopf bifurcation. We find two-dimensional nonlinear time-periodic flows that arise from these bifurcations. The disturbance to the basic flow has wavy streamlines meandering between a sequence of triangular-shaped vortices, with this pattern skewing towards the channel wall which the basic flow skews towards. For each of these secondary flows we identify a nonlinear critical Reynolds number (based on half-channel width and viscosity at one of the fixed wall temperatures) which represents the minimum Reynolds number at which a secondary flow may exist. In contrast to the results for the linear critical Reynolds number, the precise form of $\mu(T)$ is not found to be qualitatively important in determining the stability of the thermal flow relative to the isothermal flow. For the viscosity models considered here, we find that the secondary flow is destabilized relative to the corresponding isothermal flow when $\mu(T)$ decreases and vice versa. However, if we remove the bulk effect of the non-uniform change in viscosity by introducing a Reynolds number based on average viscosity, it is found that the form of $\mu(T)$ is important in determining whether the thermal secondary flow is stabilized or destabilized relative to the corresponding isothermal flow. We also consider the linear stability of the secondary flows and find that the most unstable modes are either superharmonic or subharmonic. All secondary disturbance modes are ultimately damped as the Floquet parameter in the spanwise direction increases, and the last mode to be damped is always a phase-locked subharmonic mode. None of the secondary flows is found to be stable to all secondary disturbance modes. Possible bifurcation points for tertiary flows are also identified.

1. Introduction

An early study of the linear stability of channel flow of fluid with temperature-dependent viscosity was performed by Potter & Graber (1972). They used a particular viscosity model relevant to water for which viscosity decreases as temperature increases. Having neglected any disturbance to the basic-state temperature distribution

† Present address: Department of Engineering Science, University of Oxford, Parks Road, Oxford OX1 3PJ, UK.

‡ Present address: Department of Aeronautics and Astronautics, Graduate School of Engineering, University of Kyoto, Kyoto 606-8501 Japan.

they obtained a modified fourth-order Orr–Sommerfeld equation. Upon fixing the temperature at the channel walls their numerical results indicated that the thermal effects introduced through a temperature-dependent viscosity destabilized the flow in the sense that the critical Reynolds number, R_c, decreased. Schäfer & Herwig (1993) considered an asymptotic solution to the general problem of the linear stability of channel flow of fluid with temperature-dependent viscosity in the limit of a small non-dimensional viscosity gradient with respect to temperature, K_0. Their numerical results for the problem of fixed channel wall temperatures indicated a monotonic decreasing relationship of R_c with K_0. Recently Wall & Wilson (1996) re-examined the linear stability of these channel flows for four different viscosity models but, in contrast to Potter & Graber (1972), they did not neglect perturbations to temperature, while in contrast to Schäfer & Herwig (1993), they did not assume K_0 to be small. Their results indicated that the physical instability mechanism of the thermal flows is similar to that of (isothermal) plane Poiseuille flow in the sense that the Reynolds stresses were found to peak close to the location of the critical layers, with however the layer in the half of the channel into which the basic flow had skewed being relatively more important in the process of energy transfer from the basic flow to the disturbance. Wall & Wilson (1996) found some perhaps unexpected results when comparing the behaviour of R_c between the different viscosity models. For example, using a Reynolds number based on viscosity at one of the walls, half-channel width and a velocity scale proportional to an imposed pressure gradient, they found the situation where one flow whose viscosity monotonically decreases across the channel is arbitrarily destabilized by heating whereas another flow whose viscosity monotonically decreases across the channel is found to be arbitrarily stabilized by heating.

The linear stability results for isothermal plane Poiseuille flow have been experimentally verified by Nishioka, Iida & Ichikawa (1975), and more recently by Elofsson & Alfredsson (1998). In more noisy experiments the value of R_c is considerably reduced, for example Davies & White (1928) found instability for R as low as 1000. Nishioka, Iida & Kanbayashi (1978) experimentally investigated the application of two-dimensional finite-amplitude disturbances to plane Poiseuille flow with the result of producing a rapid growth of three-dimensional spanwise structures in the flow similar to those observed by Klebanoff, Tidstrom & Sargent (1962) in boundary-layer flow. Kozlov & Ramazanov (1984) observed a similar development of three-dimensional subharmonic disturbances from two-dimensional finite-amplitude waves. Direct numerical solutions of the time-dependent Navier–Stokes equations, for example those by Orszag & Kells (1980) or Rozhdestvensky & Simakin (1984), exhibit a similar secondary growth of three-dimensional disturbances to that observed in these experiments. The present study of the thermal problem will instead consider the transition process in terms of a sequence of bifurcations of the basic flow, that is we shall perform a global numerical bifurcation analysis.

An early investigation of the flows bifurcating from plane Poiseuille flow was the 'weakly' nonlinear study performed by Meksyn & Stuart (1951). They considered a small-amplitude disturbance including a modification to the mean flow, but neglected harmonics of the fundamental disturbance. They found that a threshold amplitude existed for subcritical values of R. A subsequent numerical investigation by Grohne (1969) indicated that this approach yielded a nonlinear minimum R of 2500. Meksyn (1964) subsequently generalized the study of Meksyn & Stuart (1951) to include three-dimensional disturbances. Stuart's (1960) and Watson's (1960) weakly nonlinear approach again considered a small-amplitude expansion valid in the neighbourhood of a linear marginal point but, in contrast to Meksyn & Stuart (1951), included harmonics

of the fundamental oscillation. This approach led to the formal derivation of Landau's equation for parallel shear flows. Pekeris & Shkoller (1969) subsequently found numerical solutions for the appropriate Landau coefficients and found supercritical solutions to bifurcate from a section of the lower branch of the marginal curve and subcritical solutions to bifurcate from the rest of the marginal curve including the critical point. Herbert (1983) produced a rational method for uniquely determining the higher-order amplitude coefficients of Landau's equation and improved the region of validity of previous weakly nonlinear approaches. However, it is the contention of Ehrenstein & Koch (1991) that the main value of these weakly nonlinear studies is to provide accurate information in a neighbourhood of the bifurcation point.

With the advent of more powerful numerical techniques (in particular spectral and pseudospectral methods) and computing facilities, strongly nonlinear studies became more feasible. Pugh & Saffman (1988), Orszag & Patera (1980) and Herbert (1981) established that the rapid growth of three-dimensional waves observed in the experimental studies is due to the linear secondary instability of the two-dimensional finite-amplitude equilibria above a threshold amplitude. Using quasi-equilibria nonlinear solutions Orszag & Patera (1983) found a reduction of the minimum nonlinear R to 1000, although later Pugh & Saffman (1988) showed that the assumption made in the former study of a change in stability at the turning point of the nonlinear bifurcation branch is an oversimplification (although a neutral eigenvalue will always exist there). A summary of these studies may be found in Bayly, Orszag & Herbert (1988). More recently Ehrenstein & Koch (1989, 1991) have computed families of three-dimensional finite-amplitude secondary bifurcation solutions originating from multiple bifurcation points at the coincidence of two or more neutral phase-locked solutions which lead to a smaller nonlinear critical R. They also computed nonlinear three-dimensional primary bifurcation solutions which did not, however, lead to a reduction in nonlinear critical R compared to two-dimensional primary bifurcations.

The present nonlinear study was undertaken to provide insight into the channel flows of fluid with temperature-dependent viscosity that may be observed in practice and to more fully understand the differences in linear stability results between different viscosity models that were found by Wall & Wilson (1996). With the introduction of thermal effects through a temperature-dependent viscosity this investigation therefore extends previous numerical bifurcation studies of channel flow. In § 2 we introduce the governing equations for this problem, present the basic states and derive the perturbation equations for the primary bifurcation solutions. We recover the linear stability problem by omitting the nonlinear terms from these equations. In § 3 we review the linear stability problem, while in § 4 we proceed to calculate the two-dimensional nonlinear equilibrium solutions for two viscosity/temperature relationships. In most cases we consider solutions which bifurcate from the linear critical point. In § 5 we derive the perturbation equations for the secondary bifurcation solutions, and present results for the three-dimensional linear stability of the secondary flows by omitting the nonlinear terms in these equations. Finally, in § 6 a discussion of our results is presented.

2. Mathematical formulation

We adopt a Cartesian coordinate system whose origin is located on the centreline of the channel. The coordinates x^*, y^* and z^* represent the distances in the streamwise, transverse and cross-channel directions respectively where a star ($*$) denotes a

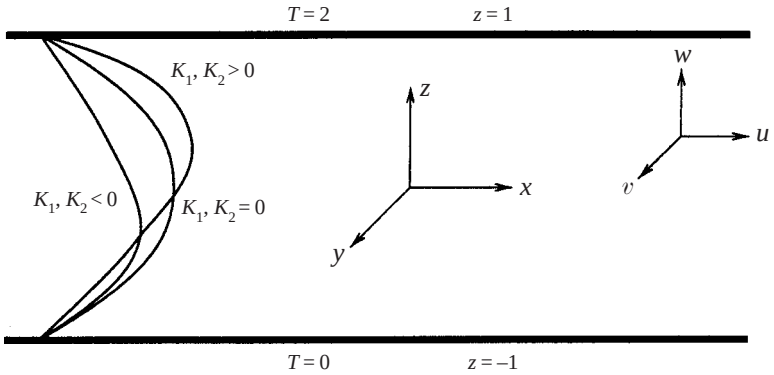

FIGURE 1. Configuration of the channel in non-dimensional coordinates.

dimensional variable. The following dimensionless variables are adopted:

$$\boldsymbol{x} = \frac{\boldsymbol{x}^*}{L}, \quad \boldsymbol{u} = \frac{\boldsymbol{u}^*}{V}, \quad p = \frac{p^*}{\rho V^2}, \quad t = t^* \frac{V}{L}, \quad \mu = \frac{\mu^*}{M}, \quad T = 2\left(\frac{T^* - T_l}{T_u - T_l}\right), \tag{1}$$

where L, ρ, M, T_u and T_l denote half the channel width, constant density, viscosity at $z^* = -L$, temperature at $z^* = L$ and temperature at $z^* = -L$ respectively. We choose the velocity scale $V = JL^2/2M$, where $-J$ $(J > 0)$ is the constant imposed pressure gradient along the channel in the positive x-direction. An illustration of the physical configuration is provided in figure 1. With this choice of dimensions our problem is governed by the non-dimensional Navier–Stokes and heat equations given by

$$\frac{\partial \boldsymbol{u}}{\partial t} + \boldsymbol{u} \cdot \nabla \boldsymbol{u} = -\nabla p + \frac{1}{R}\left\{\mu(T)\nabla^2 \boldsymbol{u} + \mu'(T)\left[2(\nabla T \cdot \nabla)\boldsymbol{u} + \nabla T \times (\nabla \times \boldsymbol{u})\right]\right\}, \tag{2}$$

$$\nabla \cdot \boldsymbol{u} = 0, \tag{3}$$

$$\frac{\partial T}{\partial t} + \boldsymbol{u} \cdot \nabla T = \frac{1}{P_e}\nabla^2 T, \tag{4}$$

subject to the following boundary conditions representing no-slip and fixed temperature at the channel walls:

$$\boldsymbol{u}(z = \pm 1) = 0, \quad T(z = -1) = 0, \quad T(z = 1) = 2. \tag{5}$$

In equations (2)–(4) $R = LV\rho/M$ is the Reynolds number and $P_e = RP_r$ is the Péclet number, where $P_r = M/\rho\kappa$ is the Prandtl number. We shall also make use of

$$\overline{R} = \frac{R}{\left(\frac{1}{2}\int_0^2 \mu(T)\mathrm{d}T\right)^2},$$

which represents a Reynolds number based on average viscosity in the channel. A basic-state solution of the form $\boldsymbol{u}(x, y, z, t) = u_0(z)\boldsymbol{i}$, $p(x, y, z, t) = p_0(x)$, $T(x, y, z, t) = T_0(z)$ is sought, where we define the unit vectors $\boldsymbol{i}, \boldsymbol{j}$ and $\boldsymbol{k}$ in the x-, y- and z-directions respectively. The boundary conditions (5) become

$$u_0(\pm 1) = 0, \quad T_0(-1) = 0, \quad T_0(1) = 2. \tag{6}$$

The basic-state temperature $T_0 = 1 + z$ is readily obtained and we are left to solve

$$R\frac{\mathrm{d}p_0}{\mathrm{d}x} = \frac{\mathrm{d}}{\mathrm{d}z}\left(\mu(T_0)\frac{\mathrm{d}u_0}{\mathrm{d}z}\right) = -2. \tag{7}$$

The general solution to equation (7) is given by

$$u_0(z) = (A - 2z)F(z) + 2\int_{-1}^{z} F(r)\,\mathrm{d}r,$$

where

$$A = \frac{2}{F(1)}(F(1) - \int_{-1}^{1} F(r)\,\mathrm{d}r)$$

and

$$F(z) = \int_{-1}^{z} \frac{\mathrm{d}r}{\mu(T_0(r))},$$

for $\mu(T(z))$ for which $F(z)$ and $\int_{-1}^{z} F(r)\,\mathrm{d}r$ exist. The present study considers two viscosity models: $\mu(T) = \mathrm{e}^{-K_1 T}$, for which

$$u_0(z) = -\frac{2}{K_1}\left[1 + \coth K_1 + (z - \coth K_1)\mathrm{e}^{K_1(1+z)}\right], \tag{8}$$

and $\mu(T) = 1 - K_2 T$ (where we require $K_2 < \frac{1}{2}$ so that $\mu(T) > 0$ everywhere) for which

$$u_0(z) = -\frac{2}{K_2}\left[\frac{-2\log\left[(1-2K_2)/(1-K_2(1+z))\right]}{\log(1-2K_2)} + 1 - z\right]. \tag{9}$$

These viscosity models, which we label 1 and 2 respectively, correspond to viscosity models 1 and 2 of Wall & Wilson's (1996) study. For both these models when $K_i > 0$, $i = 1, 2$, viscosity monotonically decreases across the channel and the basic flow skews towards the hot wall ($z = 1$), whereas when $K_i < 0$, $i = 1, 2$, viscosity monotonically increases across the channel and the basic flow skews towards the cold wall ($z = -1$). When $K_i = 0$, $i = 1, 2$, the basic flow is given by the isothermal plane Poiseuille flow. Illustrations of these basic states may be found in figure 4 as well as in Wall & Wilson (1996) and Wall (1996).

We seek a solution to the governing equations (2)–(4) subject to the boundary conditions (5) in the form

$$\boldsymbol{u} = \boldsymbol{u}_0 + \hat{\boldsymbol{u}}, \quad p = p_0 + \hat{p}, \quad T = T_0 + \hat{T},$$

and so we are left to solve

$$\begin{aligned}\frac{\partial \hat{\boldsymbol{u}}}{\partial t} + \boldsymbol{u}_0\cdot\nabla\hat{\boldsymbol{u}} + \hat{\boldsymbol{u}}\cdot\nabla\boldsymbol{u}_0 + \hat{\boldsymbol{u}}\cdot\nabla\hat{\boldsymbol{u}} = -\nabla\hat{p} + \frac{1}{R}\Big\{&\mu_D(T_0,\hat{T})\nabla^2\boldsymbol{u}_0 + \mu(T_0+\hat{T})\nabla^2\hat{\boldsymbol{u}} \\ &+ \mu'(T_0+\hat{T})[2(\nabla T_0\cdot\nabla\hat{\boldsymbol{u}} + \nabla\hat{T}\cdot\nabla\boldsymbol{u}_0 + \nabla\hat{T}\cdot\nabla\hat{\boldsymbol{u}}) + \nabla T_0\times(\nabla\times\hat{\boldsymbol{u}}) \\ &+ \nabla\hat{T}\times(\nabla\times\boldsymbol{u}_0) + \nabla\hat{T}\times(\nabla\times\hat{\boldsymbol{u}})] + \mu'_D(T_0,\hat{T})\,[2\nabla T_0\cdot\nabla\boldsymbol{u}_0 + \nabla T_0\times(\nabla\times\boldsymbol{u}_0)]\Big\},\end{aligned} \tag{10}$$

$$\nabla\cdot\hat{\boldsymbol{u}} = 0, \tag{11}$$

$$\frac{\partial\hat{T}}{\partial t} + \boldsymbol{u}_0\cdot\nabla\hat{T} + \hat{\boldsymbol{u}}\cdot\nabla T_0 + \hat{\boldsymbol{u}}\cdot\nabla\hat{T} = \frac{1}{P_e}\nabla^2\hat{T}, \tag{12}$$

subject to

$$\hat{\boldsymbol{u}}(z=\pm 1)=\boldsymbol{0}, \quad \hat{T}(z=\pm 1)=0, \tag{13}$$

where $\mu_D(T_0,\hat{T})=\mu(T_0+\hat{T})-\mu(T_0)$ and $\mu'_D(T_0,\hat{T})=\mu'(T_0+\hat{T})-\mu'(T_0)$. The present study will only consider nonlinear solutions in the limit as $P_e\to 0$ for R held constant. In this case, if we insist that $\hat{T}$ is bounded in the limit as $x, y\to\pm\infty$, we have $\hat{T}\equiv 0$. Thus we are left to solve

$$\frac{\partial\hat{\boldsymbol{u}}}{\partial t}+\boldsymbol{u}_0\cdot\nabla\hat{\boldsymbol{u}}+\hat{\boldsymbol{u}}\cdot\nabla\boldsymbol{u}_0+\hat{\boldsymbol{u}}\cdot\nabla\hat{\boldsymbol{u}} = -\nabla\hat{p}+\frac{1}{R}\left\{\mu(T_0)\nabla^2\hat{\boldsymbol{u}}+\mu'(T_0)\left[2\nabla T_0\cdot\nabla\hat{\boldsymbol{u}}+\nabla T_0\times(\nabla\times\hat{\boldsymbol{u}})\right]\right\}, \tag{14}$$

$$\nabla\cdot\hat{\boldsymbol{u}}=0. \tag{15}$$

We decompose the velocity disturbance $\hat{\boldsymbol{u}}$ according to

$$\hat{\boldsymbol{u}}=\check{U}(z,t)\boldsymbol{i}+\check{\boldsymbol{u}}, \tag{16}$$

where $\check{U}(z,t)$ represents the x–y average of $\hat{\boldsymbol{u}}$ in the x-direction. We further decompose the solenoidal fluctuating part, $\check{\boldsymbol{u}}$, of $\hat{\boldsymbol{u}}$ into poloidal and toroidal parts so that the incompressibility condition (15) is automatically satisfied,

$$\check{\boldsymbol{u}}=\nabla\times(\nabla\times\phi\boldsymbol{k})+\nabla\times\psi\boldsymbol{k}. \tag{17}$$

Substituting expressions (16) and (17) into equations (14) for $\hat{\boldsymbol{u}}$ and applying the operators $\boldsymbol{k}\cdot\nabla\times(\nabla\times$ and $\boldsymbol{k}\cdot\nabla\times$ we obtain

$$\frac{\partial(\nabla^2\Delta_2\phi)}{\partial t}+U\nabla^2\Delta_2\phi_x-\frac{\partial^2 U}{\partial z^2}\Delta_2\phi_x+\boldsymbol{k}\cdot\nabla\times(\nabla\times\check{\boldsymbol{u}}\cdot\nabla\check{\boldsymbol{u}}) = \frac{1}{R}\left\{\mu(T_0)\nabla^4\Delta_2\phi+2\mu'(T_0)\frac{\mathrm{d}T_0}{\mathrm{d}z}\nabla^2\Delta_2\phi_z + \left(\mu'(T_0)\frac{\mathrm{d}^2T_0}{\mathrm{d}z^2}+\mu''(T_0)\left(\frac{\mathrm{d}T_0}{\mathrm{d}z}\right)^2\right)(\Delta_2\phi_{zz}-\Delta_4\phi)\right\}, \tag{18}$$

$$\frac{\partial(\Delta_2\psi)}{\partial t}+U\Delta_2\psi_x-\frac{\partial U}{\partial z}\Delta_2\phi_y-\boldsymbol{k}\cdot\nabla\times\check{\boldsymbol{u}}\cdot\nabla\check{\boldsymbol{u}}=\frac{1}{R}\left\{\mu(T_0)\nabla^2\Delta_2\psi+\mu'(T_0)\frac{\mathrm{d}T_0}{\mathrm{d}z}\Delta_2\psi_z\right\}, \tag{19}$$

subject to

$$\psi(\pm 1)=\phi(\pm 1)=\left.\frac{\partial\phi}{\partial z}\right|_{z=-1}=\left.\frac{\partial\phi}{\partial z}\right|_{z=1}=0, \tag{20}$$

where $U=u_0(z)+\check{U}(z,t)$ is the mean flow and Δ_2 is the two-dimensional Laplacian, $\Delta_2=\partial^2/\partial x^2+\partial^2/\partial y^2$.

3. Linear stability

We retain the temperature perturbation, $\hat{T}$, in equations (10)–(12) in order to compare with the results of Wall & Wilson (1996) who considered non-zero values of P_e for the linear problem. In fact, Wall & Wilson (1996) found the linear primary eigenvalues to be insensitive to changes in the value of P_e, as is discussed in § 3.2. We neglect terms involving products of the disturbance, and also the mean flow distortion, $\check{U}$, in equation (16) since we are considering infinitesimally small disturbances. As

shown by Wall (1996) for example, it is easily shown that Squire's theorem for the isothermal problem, which ensures that it is sufficient to consider two-dimensional disturbances, may be extended to the thermal problem. In the context of the present problem, application of Squire's theorem means we may proceed with $\psi \equiv 0$. Seeking solutions in the normal temporal-mode form

$$\phi = \phi(z)\mathrm{e}^{\mathrm{i}\alpha(x-ct)}, \tag{21}$$

where we assume α is real and non-negative without loss of generality, we are left to solve a linear differential system of the form

$$\frac{\mathrm{i}}{R}\left[\mu(T_0)(\phi^{(4)} - 2\alpha^2\phi'' + \alpha^4\phi) + \mu'(T_0)(\mathrm{D}_1\phi + \mathrm{E}_1 T) + \mu''(T_0)(\mathrm{D}_2\phi + \mathrm{E}_2 T) + \mu'''(T_0)u_0' T_0'^2 T\right] = \alpha(c-u_0)(\phi'' - \alpha^2\phi) + \alpha\phi u_0'', \tag{22}$$

$$\mathrm{i}\alpha(u_0 - c)T - \mathrm{i}\alpha T_0'\phi = \frac{1}{P_e}(T'' - \alpha^2 T), \tag{23}$$

subject to the boundary conditions

$$\phi(z = \pm 1) = \phi'(z = \pm 1) = 0, \tag{24}$$

where the operators D_1, D_2, E_1 and E_2 may be found in Wall & Wilson (1996). Equations (22) and (23) subject to boundary conditions (24) form a linear differential eigenvalue problem for the wave speed, c, as a function of the wavenumber, α, R and P_e.

3.1. *Numerical method*

The majority of the linear stability results presented here are taken from Wall & Wilson (1996). However, some additional results were required and so the following numerical method was developed. We expand the eigenfunction as a Chebyschev series,

$$\phi(z) = \sum_{k=0}^{\infty} a_k(1-z^2)^2 T_k(z), \qquad T(z) = \sum_{k=0}^{\infty} b_k(1-z^2)T_k(z), \tag{25}$$

where $T_k(z) = \cos(k \arccos(z))$ is the kth Chebyschev polynomial and the factors $(1-z^2)^2$ and $(1-z^2)$ ensure that the boundary conditions are automatically satisfied. To obtain a numerical solution using the pseudospectral method we truncate the summation in the expansions (25) at $k = N$ and evaluate equations (22) and (23) at the $N+1$ (internal) collocation points

$$z_i = \cos\frac{\mathrm{i}\pi}{N+2}, \quad i = 1, \ldots, N+1. \tag{26}$$

We are left to solve a set of $2(N+1)$ equations for the unknown complex coefficients a_k and b_k which poses a generalized algebraic eigenvalue problem for c. We solve this eigenvalue problem using the QZ algorithm which is accomplished using NAG routine F02GJF. Calculations were made on the Sun Sparc 20 workstation and a single evaluation of the eigenvalue spectrum when $N = 60$ took around 8 seconds. For the isothermal problem when $R = 10^4$ and $\alpha = 1$, we obtain $c = 0.237526488820 + 0.003739670623\mathrm{i}$ when $N = 89$ in excellent agreement with previous authors, for example Orszag (1971) obtained $c = 0.23752649 + 0.00373967\mathrm{i} \pm 10^{-8}(1+\mathrm{i})$. We found convergence for viscosity model 2 to be slower in the limit as $K_2 \to \frac{1}{2}$ in accordance with the numerical difficulty encountered by Wall & Wilson (1996) in this limit.

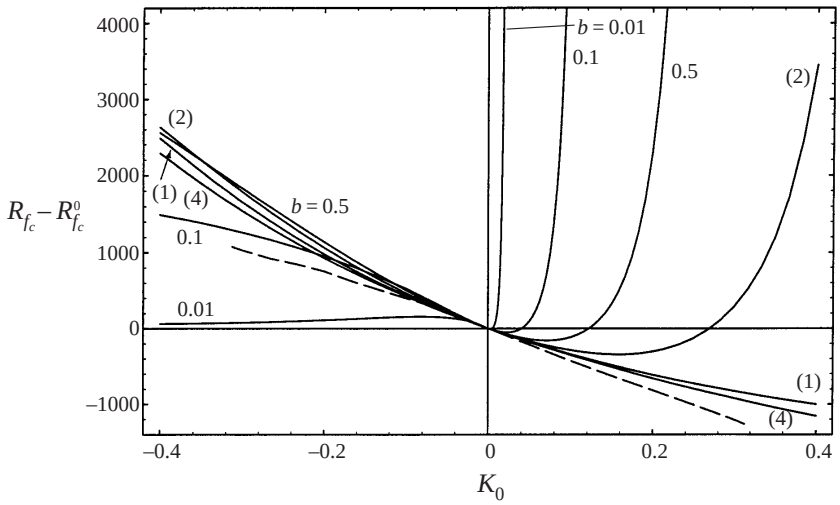

FIGURE 2. $R_{f_c} - R_{f_c}^0$ plotted as a function of K_0 when $P_e = 1$ for the four different viscosity models (1)–(4). Schäfer & Herwig's (1993) asymptotic results are shown by the dashed line.

3.2. *Results*

Wall & Wilson (1996) solved the problem given by equations (22) and (23) subject to boundary conditions (24) numerically using a high-order finite-difference technique on an irregular grid allied with the QZ algorithm. In addition to the two viscosity models of the present study, Wall & Wilson (1996) also considered the models $\mu(T) = 1 + b(1 - \mathrm{e}^{K_3 T})$ and $\mu(T) = C\mathrm{e}^{(K_4 T + F)^{-1}}$, henceforth labelled models 3 and 4 respectively. These viscosity models are also monotonic decreasing or increasing functions of temperature when $K_i > 0$ or $K_i < 0, i = 3, 4$, respectively, where $F = 0.16393$, $C = \mathrm{e}^{-1/F}$ and $b > 0$. Wall & Wilson (1996) found the instability mechanism of the thermal problem to be similar to that of the isothermal problem, with Reynolds stresses peaking close to the location of critical layers. They found, however, that for the thermal case there is a larger transfer of energy from the basic flow to the disturbance in the half of the channel into which the basic flow has deflected. In figure 2 we plot the behaviour of the change in the critical Reynolds number due to heating, $R_{f_c} - R_{f_c}^0$, against $K_0 = -\mu'(0)$ when $P_e = 1$. We have introduced the Reynolds number based on flux,

$$R_f = \frac{1}{2}\int_{-1}^{1} u_0(z)\,\mathrm{d}z\; R,$$

in order to compare results with those of Schäfer & Herwig's (1993) asymptotic study in the limit as $K_0 \to 0$ which are also plotted. The critical Reynolds number, R_c, represents the largest Reynolds number the basic flow may have while retaining its laminar form according to the linear theory. The symbol $R_{f_c}^0 = 3848.1$ denotes the value of the isothermal critical Reynolds number based on flux. This figure shows some perhaps unexpected results – for instance we have a situation where one flow whose viscosity monotonically decreases across the channel may be stabilized by heating (for example viscosity model 2) whereas another flow whose viscosity monotonically decreases across the channel is found to be always destabilized by heating (for example model 1). Wall & Wilson (1996) proposed an explanation of their results in terms

of three physical effects which they labelled bulk effects, velocity-profile shape effects and thin-layer effects.

Bulk effects describe the stabilization or destabilization of a flow that occurs when a fluid's viscosity is uniformly increased or decreased respectively. Since there is some change in average viscosity included in the non-uniform changes in viscosity for changing values of K_0, this effect is therefore stabilizing when $K_0 < 0$ and destabilizing when $K_0 > 0$. The bulk effect alone would therefore suggest a monotonic decreasing relationship of R_{f_c} with K_0 and the exceptions to this relationship must be due to other effects. In fact the bulk effect is easily filtered out of the results by plotting instead $\overline{R_c}$ against $\overline{K_0}$ where values of $\overline{K}_0(K_i)$, $i = 2,\ldots,4$, for each value of K_i, $i = 2,\ldots,4$, are found such that

$$\int_0^2 \mu(T,\overline{K}_0(K_i))\,\mathrm{d}T = \int_0^2 \mathrm{e}^{-\overline{K}_0 T}\,\mathrm{d}T, \tag{27}$$

that is for a given value of $\overline{K}_0$ the average viscosity of all models is the same. This scaling was undertaken by Wall & Wilson (1996), and their figure 15 is replotted in figure 3. Evidently all the $\overline{R_c}$ curves are flat in the neighbourhood of $\overline{K_0} = 0$ which suggests that bulk effects predominate in the limit as $\overline{K_0}$, $K_0 \to 0$ in agreement with the monotonic decreasing relationship of R_c with K_0 found by Schäfer & Herwig (1993) in the limit $K_0 \to 0$.

Velocity-profile shape effects describe the stabilization that occurs when a symmetric basic state becomes skewed (see for example the study by Potter & Smith (1968). This shape effect is thus stabilizing for both positive and negative K_0.

The third effect proposed to be relevant to the linear stability problem is an effect related to the formation of thin layers of fluid near a channel wall of differing viscosity to the fluid in the rest of the channel. Wall & Wilson's (1996) results suggested that the formation of a thin-layer of less viscous fluid adjacent to a channel wall stabilizes the flow for the present problem and vice versa. An illustration of these effects in relation to the linear problem may be found in Wall & Wilson (1996). We also note that Wall & Wilson (1996) found the linear stability characteristics of the flow to be only weakly dependent on the value of P_e in the sense that the eigenvalue spectrum was relatively insensitive to changes in the value of this parameter. Values of R_c typically changed by only a few percent for $0 \leqslant P_e \leqslant 10^5$ for the values of $\overline{K}_0$ considered.

4. Two-dimensional nonlinear equilibrium solutions

The previous section describes how the basic flow loses stability to a two-dimensional disturbance at finite values of R. In order to more fully understand the transition process, we seek to calculate the nonlinear secondary flows which bifurcate from the basic flows. Accordingly we shall seek to calculate two-dimensional solutions (i.e. with $\psi \equiv 0$) to equation (18) with the nonlinear terms included. The nonlinear terms not explicitly expressed in these equations are given in the Appendix for reference. Since the linear solutions presented by Wall & Wilson (1996) find that $c_1^R \neq 0$ on the linear marginal curves, we anticipate a Hopf bifurcation there, and accordingly seek a periodic solution in the travelling-wave form

$$\phi(x,z,t) = \sum_{l=0}^{\infty}\sum_{m=-\infty}^{\infty} a_{l,m}\mathrm{e}^{\mathrm{i}m\alpha(x-ct)}T_l(z)(1-z^2)^2, \tag{28}$$

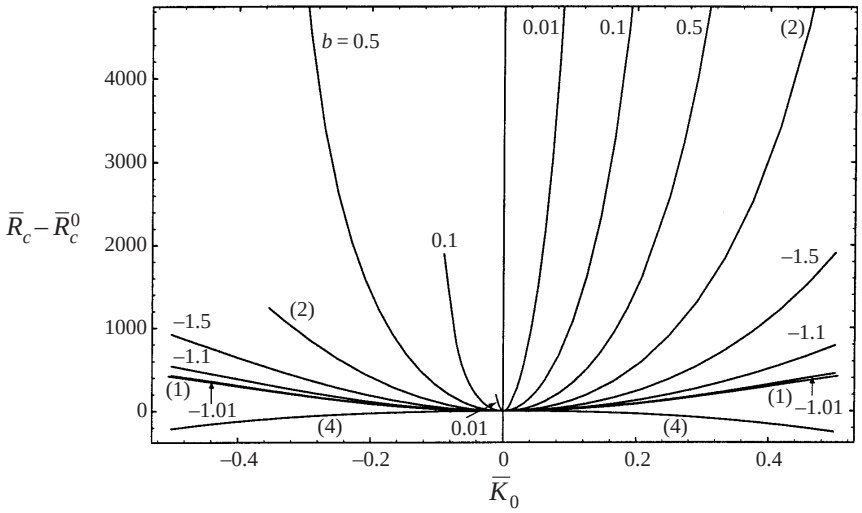

FIGURE 3. $\overline{R}_c - \overline{R}_c^0$ plotted as a function of $\overline{K}_0$ when $P_e = 1$ for the four different viscosity models (1)–(4).

where $a_{l,m}$ is complex and c is the (unknown) real wave speed. We decompose the mean flow distortion according to

$$\check{U}(z,t) = \sum_{k=0}^{\infty} C_k T_k(z)(1-z^2), \tag{29}$$

where the coefficients C_k are real. Since ϕ is real we have that $\overline{\phi} = \phi$, where $\overline{Z}$ denotes the complex conjugate of Z, so we have

$$\sum_{l=0}^{\infty}\sum_{m=\infty}^{-\infty} \overline{a_{l,-m}} \mathrm{e}^{\mathrm{i}m\alpha(x-ct)} T_l(z)(1-z^2)^2 = \sum_{l=0}^{\infty}\sum_{m=-\infty}^{\infty} a_{l,m}\mathrm{e}^{\mathrm{i}m\alpha(x-ct)} T_l(z)(1-z^2)^2,$$

and we may truncate the sum in the expression (28) to positive values of m and calculate the coefficients $\hat{a}_{l,m}$ for negative values of m *a posteriori* using the relationships

$$a^R_{l,-m} = a^R_{l,m}, \quad a^I_{l,-m} = -a^I_{l,m}.$$

Since the basic flows derived above are not symmetrical about $z = 0$, in general we cannot further reduce the number of unknowns by symmetry arguments as is the case with symmetric basic flows, see Ehrenstein & Koch (1991) for example. We choose $t = t_0$ so that the imaginary part of $a_{1,2}\mathrm{e}^{-2\mathrm{i}\alpha c t_0}$, for example, is zero and introduce the constants

$$\hat{a}_{l,m} = a_{l,m}\mathrm{e}^{-\mathrm{i}m\alpha c t_0}.$$

Taking the $x-y$ average of the x-component of equation (14), we obtain the following equation for $\check{U}$:

$$\frac{\partial \check{U}}{\partial t} - \frac{\alpha\beta}{4\pi^2}\frac{\partial}{\partial z}\int_0^{2\pi/\alpha}\int_0^{2\pi/\beta} \Delta_2\phi(\phi_{xz}+\psi_y)\,\mathrm{d}x\,\mathrm{d}y = \frac{1}{R}\left(\mu(T_0)\frac{\partial^2\check{U}}{\partial z^2} + \mu'(T_0)\frac{\mathrm{d}T_0}{\mathrm{d}z}\frac{\partial \check{U}}{\partial z}\right). \tag{30}$$

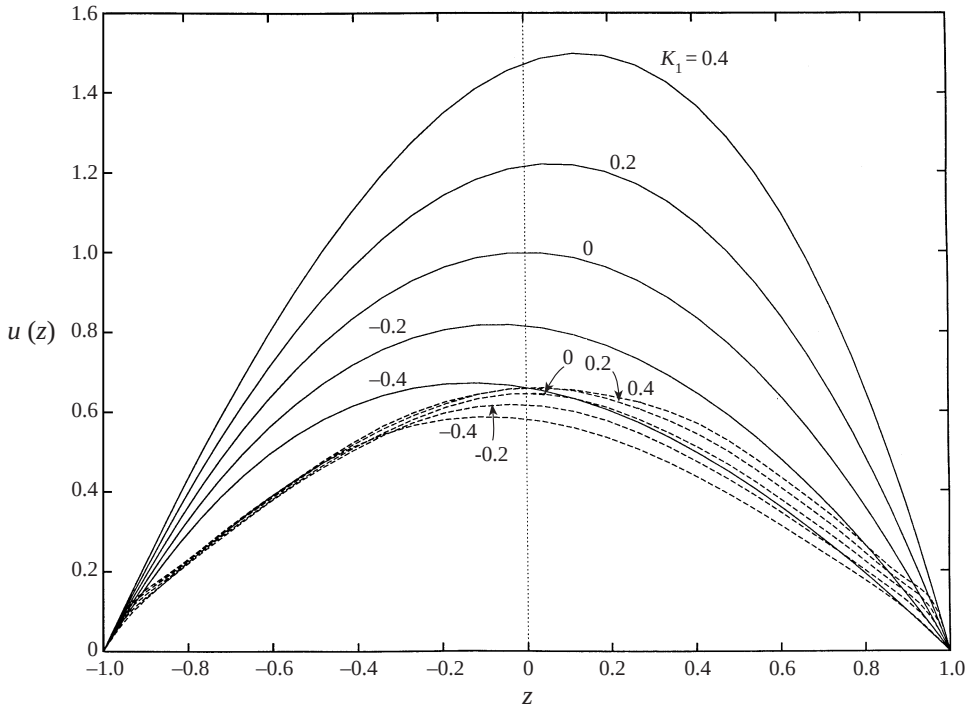

FIGURE 4. Basic states (—) and the corresponding upper-branch mean flows (- - -) for $\mu(T) = \mathrm{e}^{-K_1 T}$ for the values of K_1 indicated when $R = 11\,000$ and $\alpha = 1.05$ with $L = 39$ and $M = 4$.

Nonlinear algebraic equations are obtained for the unknown coefficients, $\hat{a}_{l,m}$, by applying the operator

$$\frac{\alpha\beta}{4\pi^2}\int_0^{2\pi/\beta} \mathrm{d}y \int_0^{2\pi/\alpha} \mathrm{d}x\, \mathrm{e}^{\mathrm{i}\gamma\alpha x}$$

to equation (18). In order to compute two-dimensional nonlinear equilibrium solutions for the present problem, our task therefore is to solve equations (18) and (30) subject to the boundary conditions (24) and $\breve{U}(z = \pm 1) = 0$.

4.1. *Numerical method*

In order to obtain numerical solutions to this problem we must truncate the series in expression (28) at $l = N$, sum m from 0 to M, and truncate the series in expression (29) at $k = K$, where in practice we always used $K = N$. We substitute these truncated series for ϕ and $\breve{U}$ in equations (18) and (30) and apply a pseudospectral method by evaluating the resultant expressions at the $N + 1$ internal collocation points given by equation (26). This leads to $(N + 1)(2M + 1)$ real nonlinear equations

$$F_n = D_{nm}X_m + H_{nmk}X_mX_k = 0, \quad n = 1, \ldots, (N + 1)(2M + 1), \tag{31}$$

where the summation convention has been used and X_m, $m = 1, \ldots, (N + 1)(2M + 1)$, represents the solution vector containing the $2(N+1)M$ unknown real and imaginary parts of the coefficients $\hat{a}_{l,m}$ and the $N + 1$ unknown real coefficients C_k, $k = 0, \ldots N$. We solve the nonlinear algebraic system of equations (31) using the Newton–Raphson iteration method. We obtain the values $\hat{a}_{01} = -0.0680754$, $c = 0.2901557$ and $\hat{a}_{01} = -0.0591568$, $c = 0.3026123$ when $M = 2$, $N = 17$ and $M = 6$, $N = 43$ respectively

K_1	I_0	I_1
−0.4	0.8182	0.8724
−0.3	0.8605	0.9142
−0.2	0.9048	0.9477
−0.1	0.9512	0.9758
0	1.0000	1.0000
0.1	1.0513	1.0214
0.2	1.1053	1.0403
0.3	1.1622	1.0561
0.4	1.2222	1.0720

TABLE 1. Measure of the skewing of basic states, I_0, and corresponding upper-branch secondary flows, I_1, when $\mu(T) = \mathrm{e}^{-K_1 T}$, $R = 11000$ and $\alpha = 1.05$.

for the upper branch of the isothermal problem when $R = 5600$ and $\alpha = 1.1$. Using $M = 2$ and $N + 1 = 15$ Ehrenstein & Koch (1991) solved this problem on half the channel with appropriate symmetry conditions along the centreline of the channel and obtained $c = 0.2878$. We define the upper and lower branches of the bifurcation curve below. In most of the subsequent work the truncation level $N = 29$, $M = 4$ was adopted. A single iteration of the Newton–Raphson method takes approximately 1 min and 40 s on the SUN SPARC 20 with this truncation level.

4.2. *Results*

One quantity of transitional flows which is of engineering interest is the mean flow, $u_0(z) + \check{U}(z)$. In figure 4 we plot basic states corresponding to viscosity model 1 for various values of K_1 and, fixing R and α, we have also plotted mean flows corresponding to the nonlinear equilibrium states for the same values of K_1. The level of skewing of the mean flow, as for the basic states, increases with increasing K_1. This is confirmed in table 1 where we display values of

$$I_1 = \frac{\int_0^1 u_0 + \check{U}\,\mathrm{d}z}{\int_{-1}^0 u_0 + \check{U}\,\mathrm{d}z}$$

for the profiles in figure 4; clearly the larger the deviation of I_1 from unity the greater the skewing. For reference we also give the corresponding values of the basic-state skew factor

$$I_0 = \frac{\int_0^1 u_0\,\mathrm{d}z}{\int_{-1}^0 u_0\,\mathrm{d}z};$$

clearly the corresponding secondary mean flows are less skewed at each value of K_1. In figure 5(*a*) we plot the L_2 norm of the $\hat{a}_{l,m}$ amplitude coefficients in parameter

FIGURE 5. (*a*) $L_2(\hat{a}_{0,1}, \ldots, \hat{a}_{N,M})$, (*b*) $\hat{a}_{0,1}$, (*c*) $\hat{a}_{1,1}$ and (*d*) c for the nonlinear periodic equilibrium states bifurcating from the laminar states at the critical point in each case for (—) $\mu(T) = \mathrm{e}^{-K_1 T}$ and (- - -) $\mu(T) = 1 - K_2 T$. The values of K_2 are chosen so that the average viscosities of both viscosity models are the same for each value of $\overline{K_0}$ indicated. In (*d*) we also plot the relationship of c with R for the linear stability problem near the bifurcation point ($\diamond$).

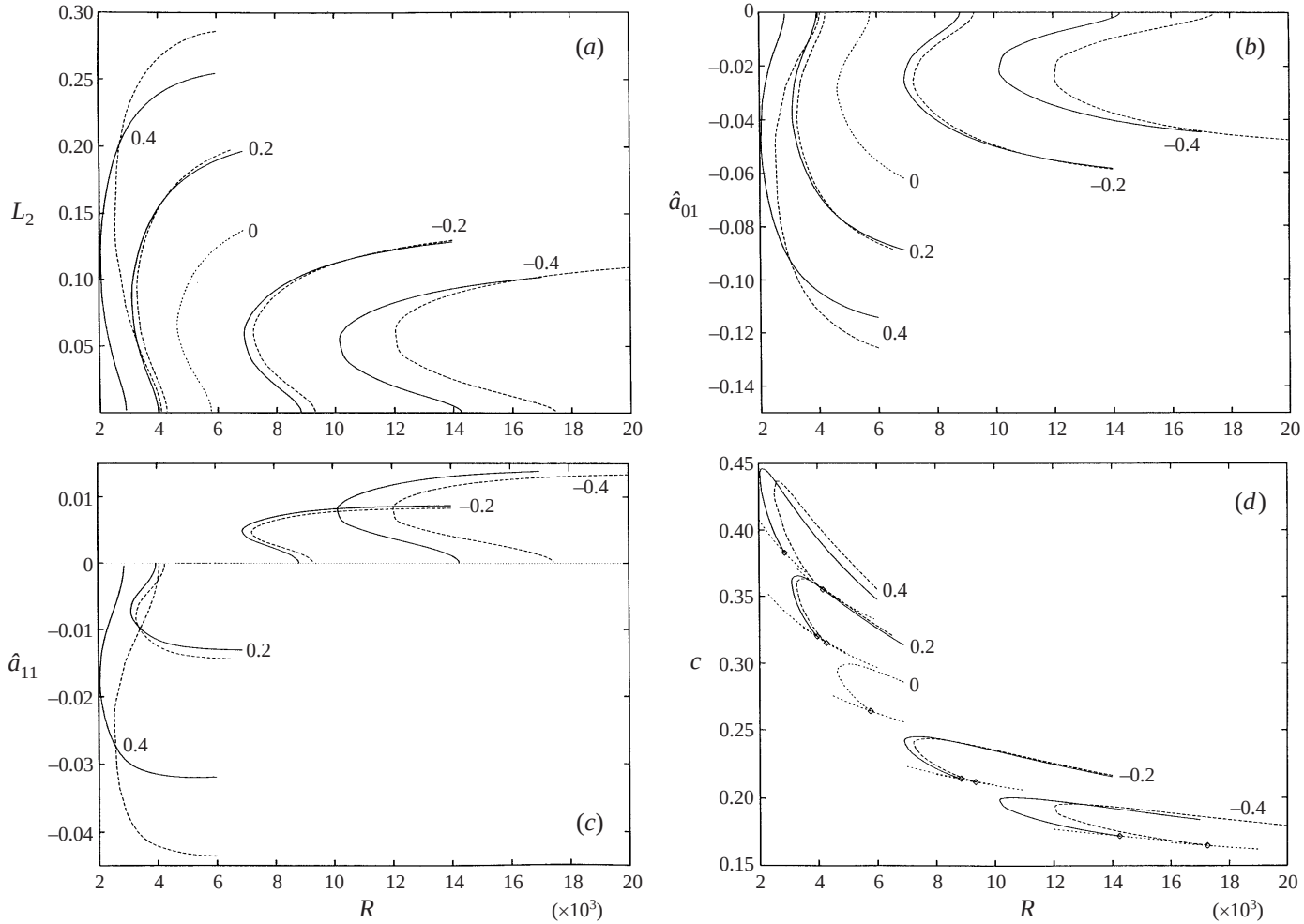

FIGURE 5. For caption see facing page.

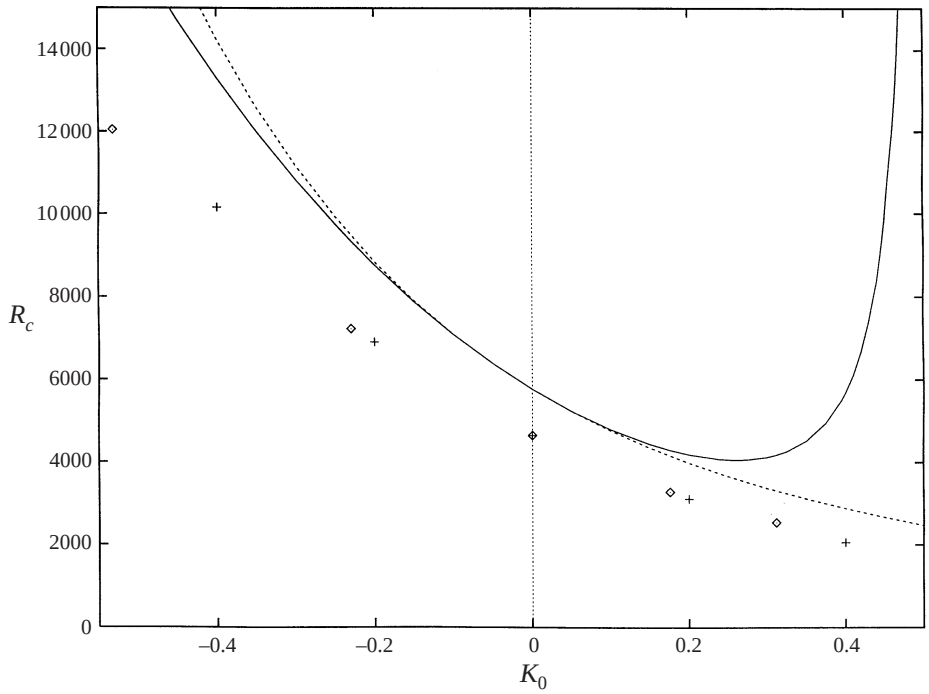

FIGURE 6. R_c plotted against K_0 for $\mu(T) = 1 - K_2 T$ (—) and $\mu(T) = \mathrm{e}^{-K_1 T}$ (- - -) together with values of R_c^{NL} for $\mu(T) = 1 - K_2 T$ ($\diamond$) and $\mu(T) = \mathrm{e}^{-K_1 T}$ (+).

space, against values of R, for both viscosity models for various values of $\overline{K_0}$. This quantity gives a measure of the amplitude of the disturbance. All the nonlinear solution branches presented in this study bifurcate from the linear critical point where $L_2(\hat{a}_{0,1}, \ldots, \hat{a}_{N,M}) = 0$. Each basic state clearly loses stability in a subcritical bifurcation. In each case, as we move away from the bifurcation point, R decreases as the amplitude of the nonlinear solution increases until a turning point is reached, and then R increases as the amplitude of the nonlinear solution increases. We denote the branch of the solution between the bifurcation point and the turning point the lower branch and the remainder of the solution branch the upper branch. The turning point may be viewed as a nonlinear critical point since it represents the smallest value of $R = R_c^{NL}$ (when $\alpha = \alpha_c$) for which a secondary flow (or primary bifurcation solution) can exist. Various values of R_c^{NL} are shown plotted in figure 6 for the two viscosity models where we also plot the corresponding linear critical Reynolds numbers, R_c. Clearly the qualitative differences in R_c between the two viscosity models are not repeated in the values of R_c^{NL}.

Wall & Wilson (1996) noted for the linear primary instability problem that the values of R_c did not coincide for different viscosity models parameterized by the same value of $\overline{K_0}$. They therefore deduced that the bulk effect (i.e. changes in average viscosity) was not sufficient by itself to explain their results. This property of the linear problem is shown in figure 5(*a*) by the different bifurcation points on the R-axis. Furthermore, the present results show that the periodic transitional flows computed here for different viscosity models for the same $\overline{K_0}$ do not converge with movement away from the bifurcation point. For a given sign of $\overline{K_0}$, the divergence of the two results is larger the larger the value of $|\overline{K_0}|$, while, for a given value of $|\overline{K_0}|$, the divergence appears to be larger for positive values of $\overline{K_0}$, which was also found to

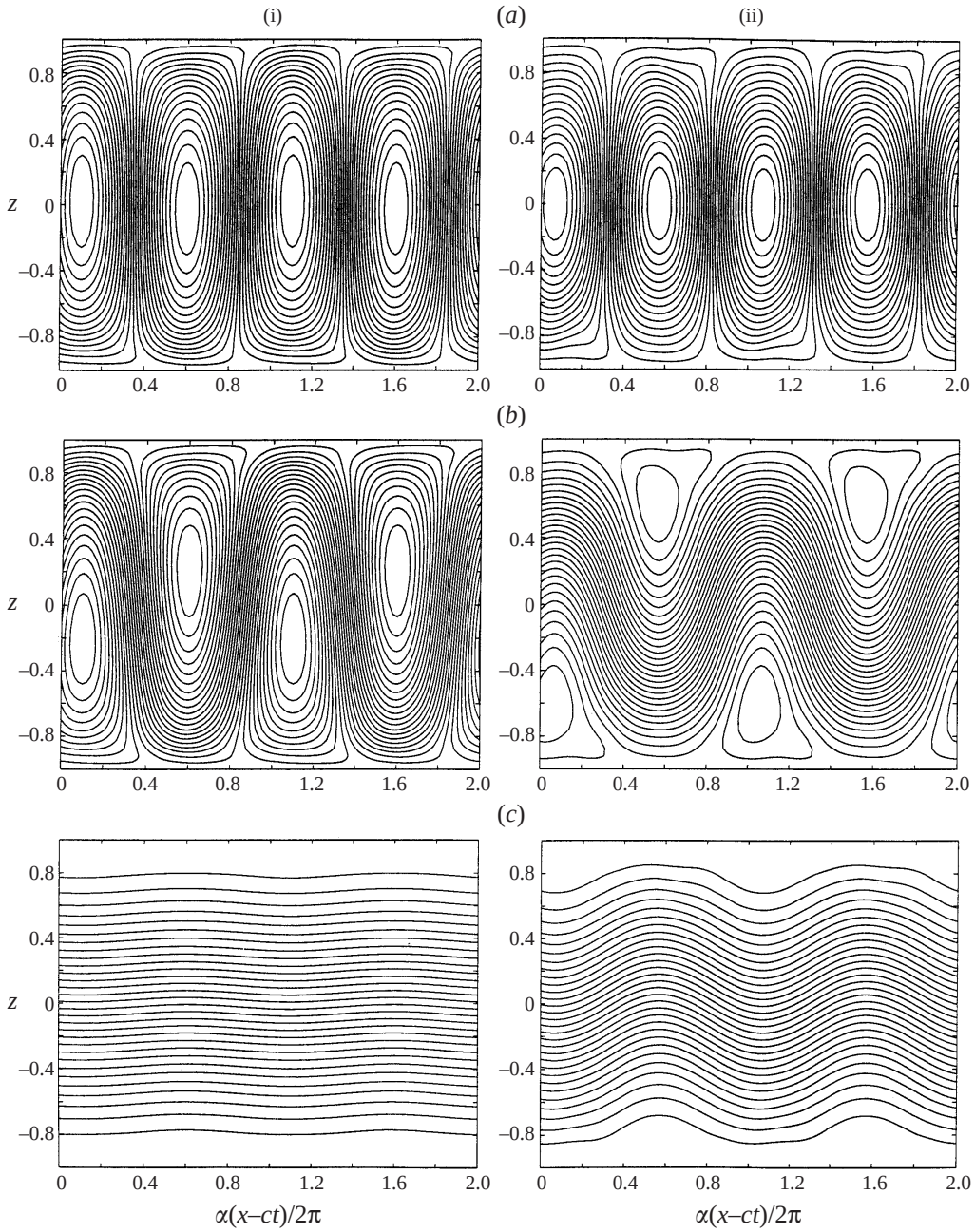

FIGURE 7. The streamfunctions (*a*) ϕ_x, (*b*) $\phi_x + \int \check{U} \mathrm{d}z$ and (*c*) $\phi_x + \int \check{U} + u_0 \mathrm{d}z$ for (i) lower-branch and (ii) upper-branch nonlinear solutions when $R = 5000$, $\alpha = 1.12$ and $K_2 = 0$. The numerical truncation level $N = 29$ and $M = 2$ was adopted in each case.

be the case for the linear primary critical point results. We also note that, for a given value of $\overline{K_0}$ and for values of R for which solutions for both viscosity models exist, the amplitude of the nonlinear solution is largest for viscosity model 2 for lower-branch solutions while the situation is reversed at the turning point. However, there then appears to be a single intersection point where the upper branches of the two solution

curves meet beyond which the nonlinear solution corresponding to viscosity model 2 once again has the larger amplitude for each value of R. In figure 5(b) we plot the leading-order even coefficient $\hat{a}_{1,0}$ against R for reference. Also, since symmetry about $z = 0$ is lost for non-zero values of $\overline{K_0}$ it is also of interest to display the corresponding plots of the leading-order odd coefficient, $\hat{a}_{1,1}$, which are shown in figure 5(c). For the isothermal problem this coefficient is identically zero, while for the thermal problem it takes the opposite sign to that of $\overline{K_0}$. The subcritical behaviour in both these figures is again clearly shown. The wave speeds corresponding to the nonlinear solutions plotted in figure 5(a–c) are plotted in figure 5(d). It should be noted that a maximum for c in general occurs at $R > R_c^{NL}$.

A visualization of the nonlinear secondary flow is provided in figures 7 and 8, where we plot the streamfunctions corresponding to the fluctuating part of the disturbance, ϕ_x, the disturbance, $\int \breve{U}\mathrm{d}z + \phi_x$, and the total flow, $(\int \breve{U} + u_0)\mathrm{d}z + \phi_x$, for $K_2 = 0$ and $K_2 = 0.3166$ respectively. With these values of K_2 the average viscosity of the corresponding basic states is identical to that of viscosity model 1 when $K_1 = 0$ and 0.4 respectively. Viewing figures 7(i)(a) and 7(ii)(a), it is clear that the fluctuating part of the disturbance on both upper and lower branches is characterized by a sequence of transverse vortices whose centres lie along $z = 0$. When the streamfunction, $\int \breve{U}\mathrm{d}z$, of the flow distortion is added to ϕ_x the combination creates a set of wavy streamlines meandering between a sequence of triangular-shaped vortices whose centres lie either side of $z = 0$ as may be seen in figures 7(i)(b) and 7(ii)(b). These figures may be compared with figure 7 of Ehrenstein & Koch's (1991) study. Clearly the $\int \breve{U}\mathrm{d}z$ term is relatively more dominant for the upper-branch solution and severely diminishes the triangular-shaped vortices. With regard to the streamlines for the total flow shown in figures 7(i)(c) and 7(ii)(c), it is clear that the straight streamlines for plane Poiseuille flow are modified for both solution branches by the introduction of a waviness, with this waviness being much larger for the upper-branch solution as may have been expected due to the higher amplitude of the nonlinear solution there.

With regard to figure 8(i)(a), it may be seen that the introduction of thermal effects has not destroyed the transverse vortical pattern found for ϕ_x for the isothermal problem, but for $K_2 > 0$ it has shifted the vortices towards the hot wall, $z = 1$. Interestingly, this shift appears to be larger for the lower-branch solutions shown in figure 8(i)(a) than for the upper-branch solutions. The pattern of streamlines corresponding to the total disturbance for the thermal problem shown in figures 8(i)(b) and 8(ii)(b) is similar to that of the isothermal problem, with again the vortices shifted towards the hot wall. Indeed for the example shown in figure 8(i)(b), the set of vortices observed to lie in the cold side of the channel for the isothermal problem now lie above the centreline. The streamlines corresponding to the total flow shown in figures 8(i)(c) and 8(ii)(c) take the same wavy form observed for the isothermal problem, with again the upper-branch streamlines exhibiting a larger-amplitude modification from the basic state. For the case when $K_2 < 0$, the change in the streamline patterns caused by the introduction of heating are of the same nature as those for $K_2 > 0$ and so are not shown here. The vortices are shifted towards the cold wall, $z = -1$, in this case. The corresponding streamfunction patterns for viscosity model 1 are qualitatively similar and so are not shown here.

5. Stability of the secondary flow

In the previous section we computed the periodic secondary flows which arise from a bifurcation of the basic states at marginal stability. It is of interest to determine

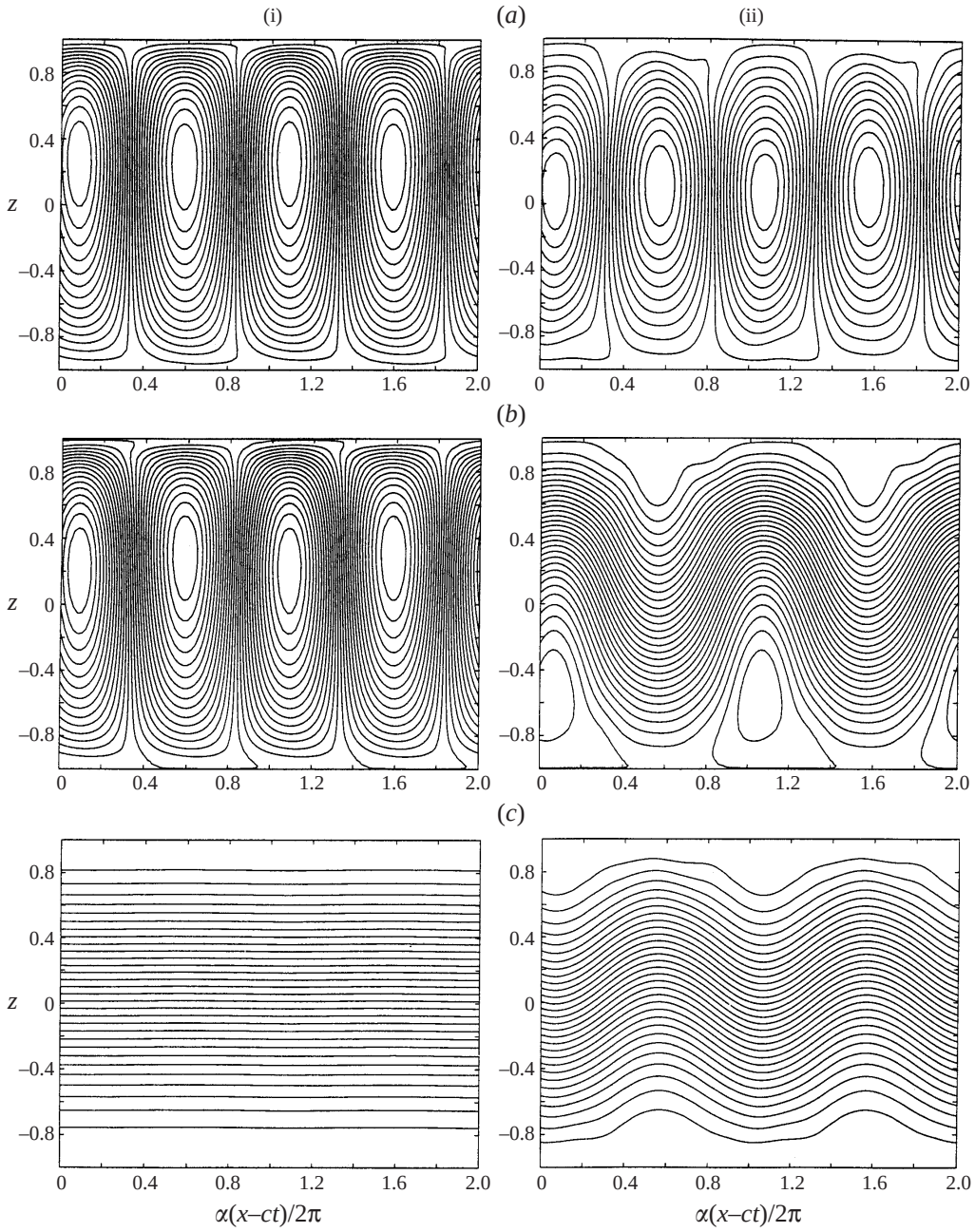

FIGURE 8. As figure 7 but when $R = 4000$, $\alpha = 0.985$ and $K_2 = 0.3166$ ($\overline{K_0} = 0.4$). The numerical truncation level $N = 29$ and $M = 4$ was adopted in each case.

the linear stability of these nonlinear secondary flows in order to give information on which of these flows may be observed in practice. In contrast to the problem of determining the linear stability of the primary flow, Squire's theorem does not apply to the secondary stability problem, and so we must consider a three-dimensional

disturbance, $\boldsymbol{u} = \tilde{\boldsymbol{u}}(x, y, z, t)$ and $p = \tilde{p}(x, y, z, t)$. The total flow

$$\boldsymbol{u} = U_0\boldsymbol{i} + \hat{\boldsymbol{u}} + \tilde{\boldsymbol{u}}, \quad p = p_0 + \hat{p} + \tilde{p}, \quad T = T_0 + \hat{T} + \tilde{T},$$

must satisfy the governing equations (2)–(4), and so

$$\begin{aligned}
&\frac{\partial \tilde{\boldsymbol{u}}}{\partial t} + \boldsymbol{u}_0 \cdot \nabla\tilde{\boldsymbol{u}} + \hat{\boldsymbol{u}} \cdot \nabla\tilde{\boldsymbol{u}} + \tilde{\boldsymbol{u}} \cdot \nabla\boldsymbol{u}_0 + \tilde{\boldsymbol{u}} \cdot \nabla\hat{\boldsymbol{u}} + \tilde{\boldsymbol{u}} \cdot \nabla\tilde{\boldsymbol{u}} \\
&\quad = -\nabla\tilde{p} + \frac{1}{R}\Bigg\{\mu\nabla^2\tilde{\boldsymbol{u}} + \mu_{DD}\nabla^2(\boldsymbol{u}_0 + \hat{\boldsymbol{u}}) + \frac{\mathrm{d}\mu}{\mathrm{d}T}\big[2(\nabla T_0 \cdot \nabla\tilde{\boldsymbol{u}} + \nabla\hat{T} \cdot \nabla\tilde{\boldsymbol{u}} \\
&\qquad + \nabla\tilde{T} \cdot \nabla\boldsymbol{u}_0 + \nabla\tilde{T} \cdot \nabla\hat{\boldsymbol{u}} + \nabla\tilde{T} \cdot \nabla\tilde{\boldsymbol{u}}) + \nabla T_0 \times (\nabla \times \tilde{\boldsymbol{u}}) + \nabla\hat{T} \times (\nabla \times \tilde{\boldsymbol{u}}) \\
&\qquad + \nabla\tilde{T} \times (\nabla \times \boldsymbol{u}_0) + \nabla\tilde{T} \times (\nabla \times \hat{\boldsymbol{u}}) + \nabla\tilde{T} \times (\nabla \times \tilde{\boldsymbol{u}})\big] + \mu'_{DD}[2(\nabla T_0 \cdot \nabla(\boldsymbol{u}_0 + \hat{\boldsymbol{u}}) \\
&\qquad + \nabla\hat{T} \cdot \nabla(\boldsymbol{u}_0 + \hat{\boldsymbol{u}})) + \nabla(T_0 + \hat{T}) \times (\nabla \times (\boldsymbol{u}_0 + \hat{\boldsymbol{u}}))]\Bigg\},
\end{aligned} \tag{32}$$

$$\nabla \cdot \tilde{\boldsymbol{u}} = 0, \tag{33}$$

$$\frac{\partial \tilde{T}}{\partial t} + \boldsymbol{u}_0 \cdot \nabla\tilde{T} + \hat{\boldsymbol{u}} \cdot \nabla\tilde{T} + \tilde{\boldsymbol{u}} \cdot \nabla T_0 + \tilde{\boldsymbol{u}} \cdot \nabla\hat{T} + \tilde{\boldsymbol{u}} \cdot \nabla\tilde{T} = \frac{1}{P_e}\nabla^2\tilde{T}, \tag{34}$$

subject to the boundary conditions

$$\tilde{\boldsymbol{u}}(z = \pm 1) = \boldsymbol{0}, \quad \tilde{T}(z = \pm 1) = 0, \tag{35}$$

where $\mu_{DD} = \mu(T_0 + \hat{T} + \tilde{T}) - \mu(T_0 + \hat{T})$, $\mu'_{DD} = \mu'(T_0 + \hat{T} + \tilde{T}) - \mu'(T_0 + \hat{T})$ and μ and $\mathrm{d}\mu/\mathrm{d}T$ are evaluated at $T = T_0 + \hat{T} + \tilde{T}$. Again examining the limit as $P_e \to 0$ for fixed R, we have $\hat{T} \equiv \tilde{T} \equiv 0$ and we are left to solve

$$\begin{aligned}
&\frac{\partial \tilde{\boldsymbol{u}}}{\partial t} + U\boldsymbol{i} \cdot \nabla\tilde{\boldsymbol{u}} + \tilde{\boldsymbol{u}} \cdot \nabla U\boldsymbol{i} + \check{\boldsymbol{u}} \cdot \nabla\tilde{\boldsymbol{u}} + \tilde{\boldsymbol{u}} \cdot \nabla\check{\boldsymbol{u}} + \tilde{\boldsymbol{u}} \cdot \nabla\tilde{\boldsymbol{u}} \\
&\qquad = -\nabla\tilde{p} + \frac{1}{R}\Bigg\{\mu\nabla^2\tilde{\boldsymbol{u}} + \frac{\mathrm{d}\mu}{\mathrm{d}T}[2\nabla T_0 \cdot \nabla\tilde{\boldsymbol{u}} + \nabla T_0 \times (\nabla \times \tilde{\boldsymbol{u}})]\Bigg\},
\end{aligned} \tag{36}$$

$$\nabla \cdot \tilde{\boldsymbol{u}} = 0, \tag{37}$$

subject to $\tilde{\boldsymbol{u}}(z = \pm 1) = \boldsymbol{0}$, where $U\boldsymbol{i} = \boldsymbol{u}_0 + \check{U}\boldsymbol{i}$. Since the disturbance is solenoidal we may decompose it according to

$$\tilde{\boldsymbol{u}} = \nabla \times (\nabla \times \tilde{\phi}\boldsymbol{k}) + \nabla \times \tilde{\psi}\boldsymbol{k},$$

so that equation (37) is automatically satisfied, and apply the operators $\boldsymbol{k} \cdot \nabla\times$ and $\boldsymbol{k} \cdot \nabla \times (\nabla\times$ as before. It may be noted that, with the exception of the terms

$$\check{\boldsymbol{u}} \cdot \nabla\tilde{\boldsymbol{u}} + \tilde{\boldsymbol{u}} \cdot \nabla\check{\boldsymbol{u}}, \tag{38}$$

equation (36) is trivially obtained from equation (14) by replacing $\boldsymbol{u}_0$ by $U\boldsymbol{i}$ and substituting $\boldsymbol{u}$ and p for $\hat{\boldsymbol{u}}$ and $\hat{p}$ respectively. The terms (38) represent the interaction between the fluctuating part of the secondary flow, $\check{\boldsymbol{u}}$, and the disturbance, $\tilde{\boldsymbol{u}}$. Since we are concerned here with the linear stability of the secondary flow, the $\tilde{\boldsymbol{u}} \cdot \nabla\tilde{\boldsymbol{u}}$ term in equation (36) is discarded, and we seek solutions in the form

$$\tilde{\phi} = \sum_{l=0}^{\infty} \sum_{m=-\infty}^{m=\infty} \tilde{a}_{l,m} \mathrm{e}^{\mathrm{i}m\alpha(x-ct) + \mathrm{i}d(x-ct) + \mathrm{i}by + \sigma t} T_l(z)(1 - z^2)^2, \tag{39}$$

$$\tilde{\psi} = \sum_{l=0}^{\infty} \sum_{m=-\infty}^{m=\infty} \tilde{b}_{l,m} \mathrm{e}^{\mathrm{i}m\alpha(x-ct)+\mathrm{i}d(x-ct)+\mathrm{i}by+\sigma t} T_l(z)(1-z^2), \tag{40}$$

where d and b are real Floquet parameters and σ is the disturbance growth rate. For given values of R, α, K_1 or K_2, d and b; if $\sigma_1^R > 0$ the flow is unstable, while if $\sigma_1^R < 0$ the flow is stable, where σ_i^R and σ_i^I denote the real and imaginary parts of the eigenvalue with the ith largest real part. If $\sigma_1^R = 0$ the flow is neutrally stable and these points offer a possible bifurcation point for the tertiary flow. We note that

$$\tilde{\phi}(b, d+\alpha) = \sum_{l=0}^{\infty} \sum_{m=-\infty}^{\infty} \tilde{a}_{l,m} \mathrm{e}^{\mathrm{i}(x-ct)[(m+1)\alpha+d]} \mathrm{e}^{\mathrm{i}by+\sigma t} T_l(z)(1-z^2)^2, \tag{41}$$

so that

$$\tilde{\phi}(b, d+\alpha) = \sum_{l=0}^{\infty} \sum_{m=-\infty}^{\infty} \tilde{a}_{l,m} \mathrm{e}^{\mathrm{i}(x-ct)[m\alpha+d]} \mathrm{e}^{\mathrm{i}by+\sigma t} T_l(z)(1-z^2)^2 = \tilde{\phi}(b, d). \tag{42}$$

The same property holds for $\tilde{\psi}$, and so the secondary perturbation is periodic in the Floquet parameter d with period α. It is therefore necessary and sufficient to examine the semi-infinite strip $0 \leqslant d < \alpha$ in Floquet parameter space at each point on the secondary-flow bifurcation branch in order to determine the stability of the secondary flow at that point. We substitute into the two equations derived from applying $\boldsymbol{k} \cdot \nabla \times$ and $\boldsymbol{k} \cdot \nabla \times (\nabla \times$ to equations (36) for $\tilde{\phi}$ and $\tilde{\psi}$ using expressions (39) and (40) and introduce

$$\tilde{\tilde{a}}_{l,m} = \tilde{a}_{l,m} \mathrm{e}^{-\mathrm{i}ct(m\alpha+d)}, \tag{43}$$

$$\tilde{\tilde{b}}_{l,m} = \tilde{b}_{l,m} \mathrm{e}^{-\mathrm{i}ct(m\alpha+d)}. \tag{44}$$

Finally we apply the operator

$$\frac{\alpha\beta}{4\pi^2} \mathrm{e}^{-\sigma t} \int_0^{2\pi/\beta} \mathrm{d}y \, \mathrm{e}^{-iby} \cdot \int_0^{2\pi/\alpha} \mathrm{d}x \, \mathrm{e}^{-i\{\gamma\alpha x+dx\}},$$

at the time $t = t_0$ defined in § 4.

5.1. *Numerical method*

Upon varying γ over the values $-M$, $-M+1, \ldots, M$ and evaluating the resultant equations at the $N+1$ internal collocation points given by equation (26), we obtain a system of $2(N+1)(2M+1)$ equations which form a generalized algebraic eigenvalue problem of the form

$$\boldsymbol{A}\boldsymbol{x} = \sigma \boldsymbol{B}\boldsymbol{x},$$

for the eigenvalues σ with eigenvector

$$(\tilde{\tilde{a}}_{0,-M}, \tilde{\tilde{a}}_{0,-M+1}, \ldots, \tilde{\tilde{a}}_{0,M}, \tilde{\tilde{a}}_{1,-M}, \ldots, \tilde{\tilde{a}}_{N,M}, \tilde{\tilde{b}}_{0,-M}, \ldots, \tilde{\tilde{b}}_{N,M}).$$

We solve this eigenvalue problem using the QZ algorithm implemented by using NAG routine F02GJF. Table 2 illustrates the convergence and modal dependence of the scheme; for most of our results we used $N = 29$ and $M = 4$.

5.2. *Results*

In figure 9 we plot contours of constant σ_1^R in the (d, b)-plane when $K_2 = -0.53$ and $\alpha = \alpha_c$ at various points along the bifurcation branch. All the secondary flows presented in § 4 are unstable for some region in the (d, b)-plane, and so none of these flows

N	M	O	σ_O^R	σ_O^I	N	M	O	σ_O^R	σ_O^I
29	4	1	0.129570	$O(10^{-14})$	39	5	1	0.131008	$O(10^{-13})$
		2	0.129154	$O(10^{-14})$			2	0.130515	$O(10^{-14})$
		3	0.111416	0.181840			3	0.115331	0.186255
		4	0.111416	−0.181840			4	0.115331	−0.186255
29	5	1	0.130578	$O(10^{-14})$	39	6	1	0.130325	$O(10^{-13})$
		2	0.130086	$O(10^{-13})$			2	0.129853	$O(10^{-14})$
		3	0.114291	0.185719			3	0.114653	−0.185289
		4	0.114291	−0.185719			4	0.114653	0.185289
29	6	1	0.129471	$O(10^{-13})$	49	4	1	0.130222	$O(10^{-13})$
		2	0.129047	$O(10^{-14})$			2	0.129792	$O(10^{-13})$
		3	0.113635	0.183290			3	0.112248	0.182874
		4	0.113635	−0.183290			4	0.112248	−0.182874
39	4	1	0.130217	$O(10^{-13})$	49	5	1	0.131020	$O(10^{-14})$
		2	0.129787	$O(10^{-14})$			2	0.130526	$O(10^{-13})$
		3	0.112246	0.182867			3	0.115329	−0.186289
		4	0.112246	−0.182867			4	0.115329	0.186289

TABLE 2. Convergence of the four most unstable superharmonic linear secondary disturbances for various values of N and M for an upper-branch isothermal nonlinear equilibrium solution when $R = 5000$, $\alpha = \alpha_c^0$ and $b = 2.5$.

may be expected to exist in equilibrium in practice since the secondary disturbance will in general be composed of all wavelengths. However, a study of the stability of these flows is nonetheless important, since it determines where the tertiary flows may bifurcate from, and yields some information on the nature of these bifurcating flows. In figure 9 some possible bifurcation points for the tertiary flow are shown by the $\sigma_1^R = 0$ contours. As table 2 demonstrates for the isothermal case, it is clear from this figure that typical growth rates of the secondary disturbance are $O(10^{-1})$ for the thermal case, and so we would anticipate a rapid growth of these disturbances similar to that found for the isothermal flow. Note that the contours are not perfectly symmetrical about $d = \alpha/2$ because we have truncated the summation in expressions (39) and (40) at finite M. Our results suggest, however, that the most unstable mode is always either the superharmonic ($d = 0$) or subharmonic ($d = \alpha/2$) mode.

In figures 10 and 11 we have plotted the real parts of the leading-order super- and subharmonic modes together with the imaginary parts of the two most unstable super- and subharmonic modes against b for secondary flows corresponding to a positive and negative value of K_2. The (a) parts of these figures permit the identification of possible bifurcation points for the tertiary flow, while the (b) parts give information on what type of flow this tertiary flow will be. For example, from figure 10 we observe that the leading-order superharmonic mode is phase locked for b up to approximately 12.5, where there is a coincidence of superharmonic modes beyond which the two most unstable superharmonic modes are given by a complex conjugate pair. We would therefore anticipate a quasi-periodic flow to bifurcate from the point at $b \approx 21.5$ where these modes cross the $\sigma^R = 0$ axis. A similar transition from a single phase-locked mode to a complex-conjugate pair of superharmonic modes may be seen in figure 11 at $b \approx 9.3$. Clearly for some values of b the most unstable mode is superharmonic while for other values of b it is subharmonic. We note that all modes are ultimately damped as b increases (the wavelength of the disturbance in the spanwise direction decreases) and the last mode to be damped is always a phase-locked subharmonic mode for the cases

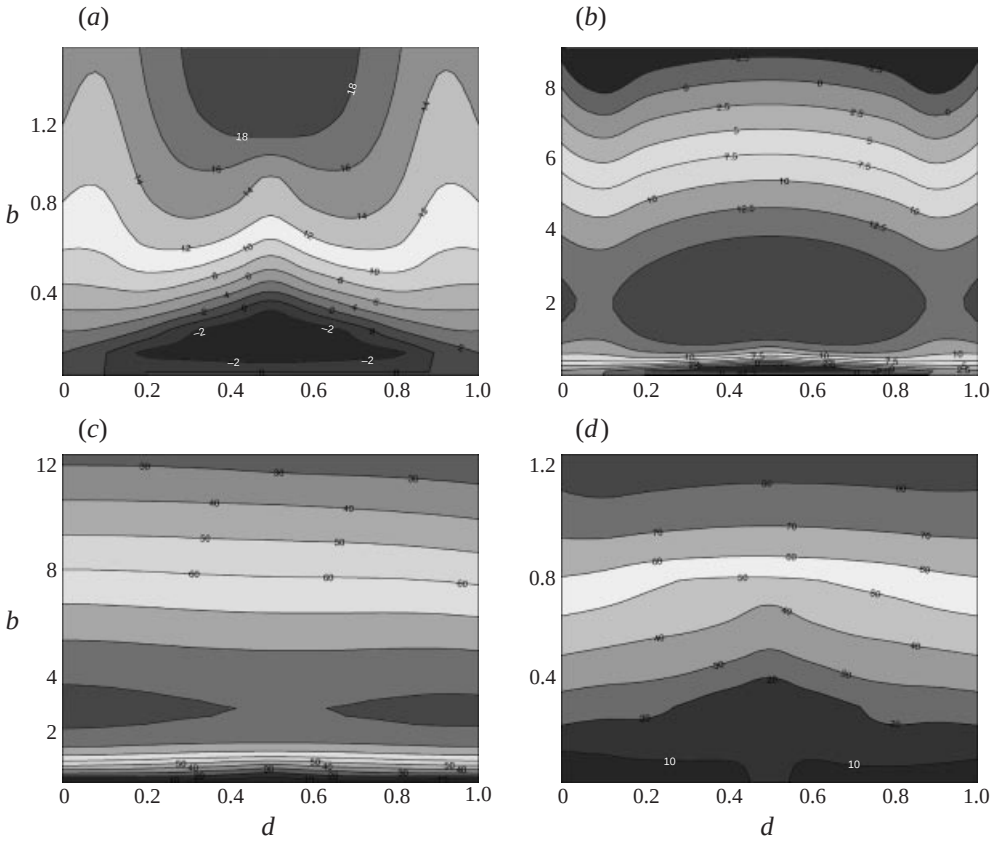

FIGURE 9. Contours of equal $\sigma_1^R \times 10^3$ for (*a*) and (*b*) lower branch $R = 16000$, (*c*) lower branch $R = 12050$ and (*d*) upper branch $R = 17000$ when $\alpha = \alpha_c = 0.998$ and $\mu(T) = 1 - K_2 T$ with $K_2 = -0.5319$.

we have considered. The value of b at which this latter stabilization occurs is larger the further along a particular bifurcation curve the secondary flow is taken from.

6. Summary

In this study we have computed the periodic secondary flows of fluid with temperature-dependent viscosity through a parallel-sided channel with fixed wall temperatures for two different viscosity/temperature relationships. These flows arise from a Hopf bifurcation of the basic flows at the linear critical point ($\alpha = \alpha_c,\ R = R_c$). We have also considered the linear stability of these secondary flows, and identified possible bifurcation points for tertiary flows.

Our results for the isothermal problem for secondary flows bifurcating from plane Poiseuille flow are in good agreement with those found by the previous studies of Ehrenstein & Koch (1989, 1991). For both the thermal and isothermal problems the bifurcation is always subcritical, with a minimum nonlinear $R = R_c^{NL}$ (i.e. a nonlinear critical Reynolds number) being reached and thence R increasing with the amplitude of the disturbance. The disturbance to the basic flow has wavy streamlines meandering between a sequence of triangular-shaped vortices with this pattern skewing towards the hot or cold wall depending on whether K_1 and K_2 are positive or negative respectively.

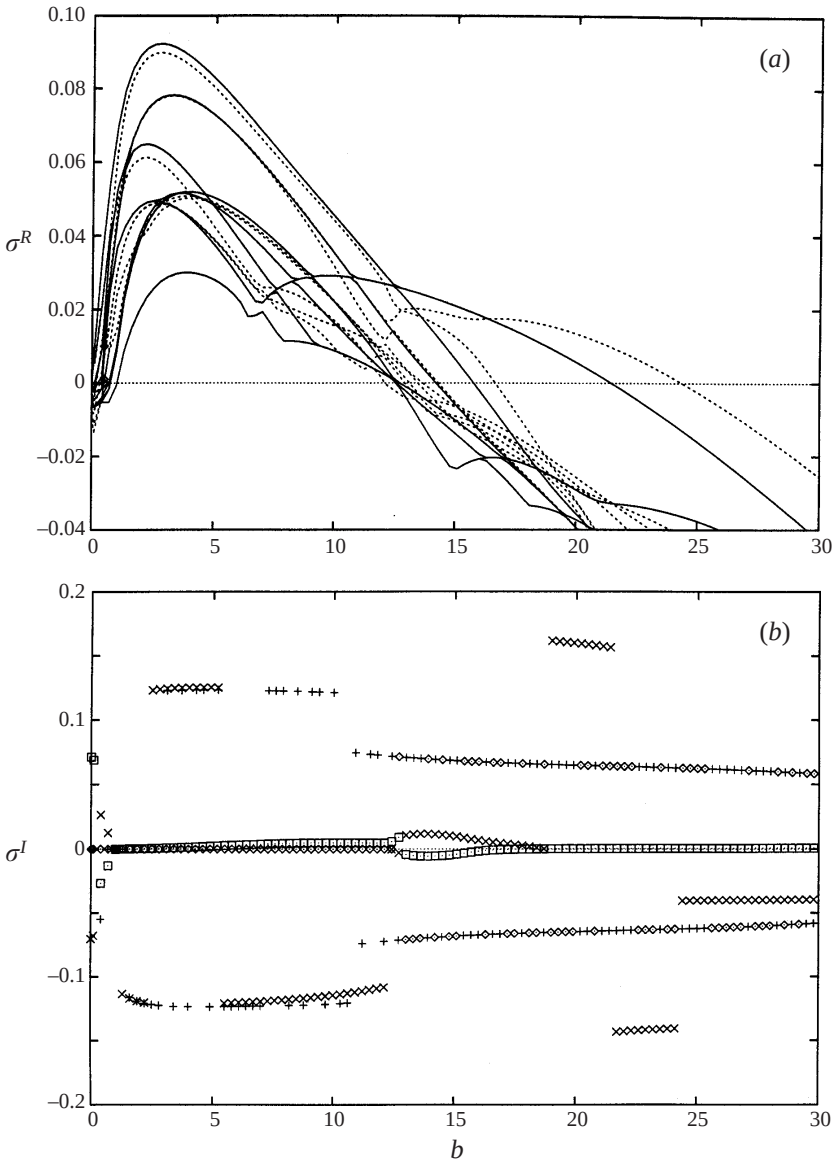

FIGURE 10. Traces of (*a*) the real part of the leading-order superharmonic (—) and subharmonic (- - -) eigenmodes and (*b*) the corresponding imaginary part of the 2 most unstable superharmonic (most unstable (◇), second most unstable (+)) and subharmonic (most unstable (□), second most unstable (×)) eigenmodes plotted against b for $\mu(T) = 1 - K_2 T$ when $K_2 = -0.53$, $R = 12050$ and $\alpha = \alpha_c$ on the lower branch.

For both viscosity models the behaviour of R_c^{NL} with K_0 is qualitatively the same, with R_c^{NL} monotonically decreasing with increasing K_0. Analysing the stability of these flows, we found that the most unstable modes are either superharmonic or subharmonic, with both types of modes being damped as the Floquet parameter in the spanwise direction increases. The last mode to be damped is always a phase-locked subharmonic mode which, at its stabilization, provides one possible bifurcation point for tertiary flows.

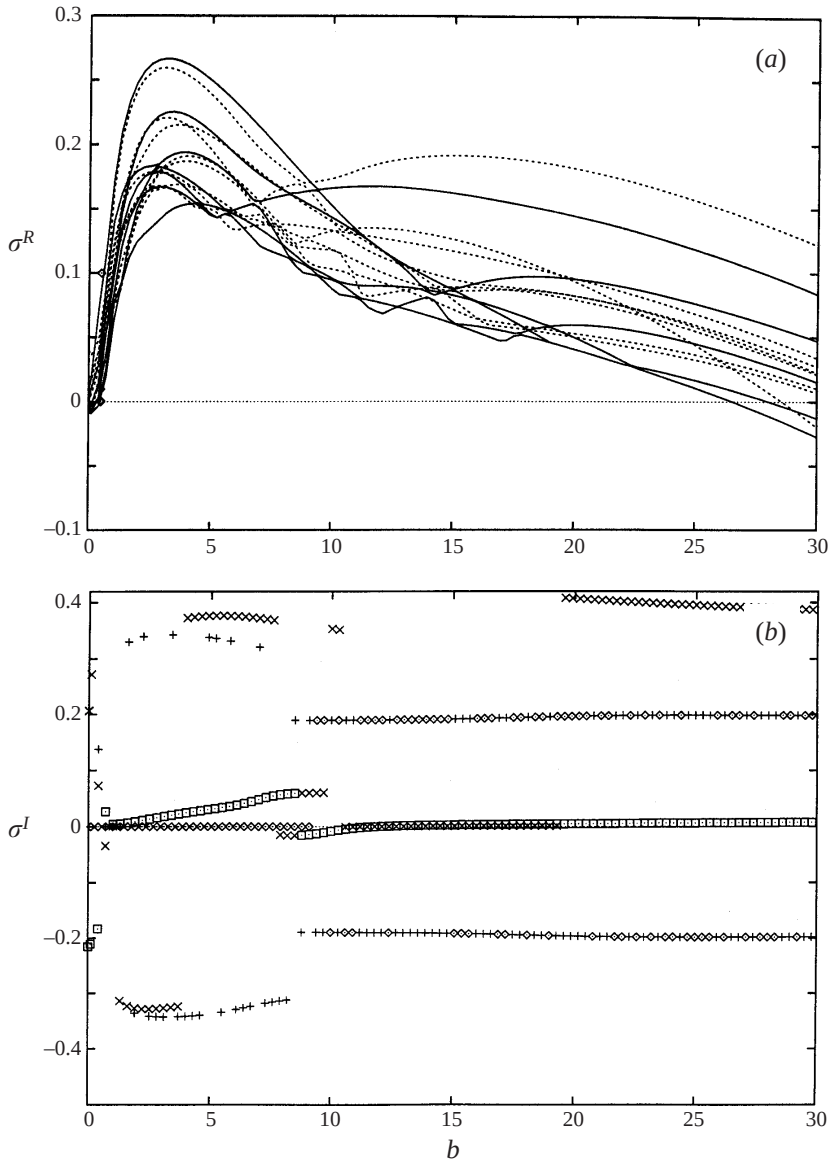

FIGURE 11. As figure 10 but for $K_2 = 0.31,\ R = 3500, \alpha = \alpha_c$ on the upper branch.

We note that the behaviour of R_c^{NL} with $K_0 > 0$ is clearly in contrast to the behaviour of R_c with $K_0 > 0$ for the two viscosity models as described by Wall & Wilson (1996) and plotted in figure 6. They found that the basic flow corresponding to viscosity model 1 was increasingly destabilized relative to plane Poiseuille flow as K_0 increased, while the basic flow corresponding to viscosity model 2, although initially destabilized relative to plane Poiseuille flow, ultimately became stabilized relative to the isothermal flow beyond a finite value of K_0. In contrast, the present nonlinear results for R_c^{NL} suggest that the form of $\mu(T)$ is not qualitatively important in determining the stability of the flow relative to the isothermal problem. In practice, isothermal channel flows with a noisy background lose stability at Reynolds number

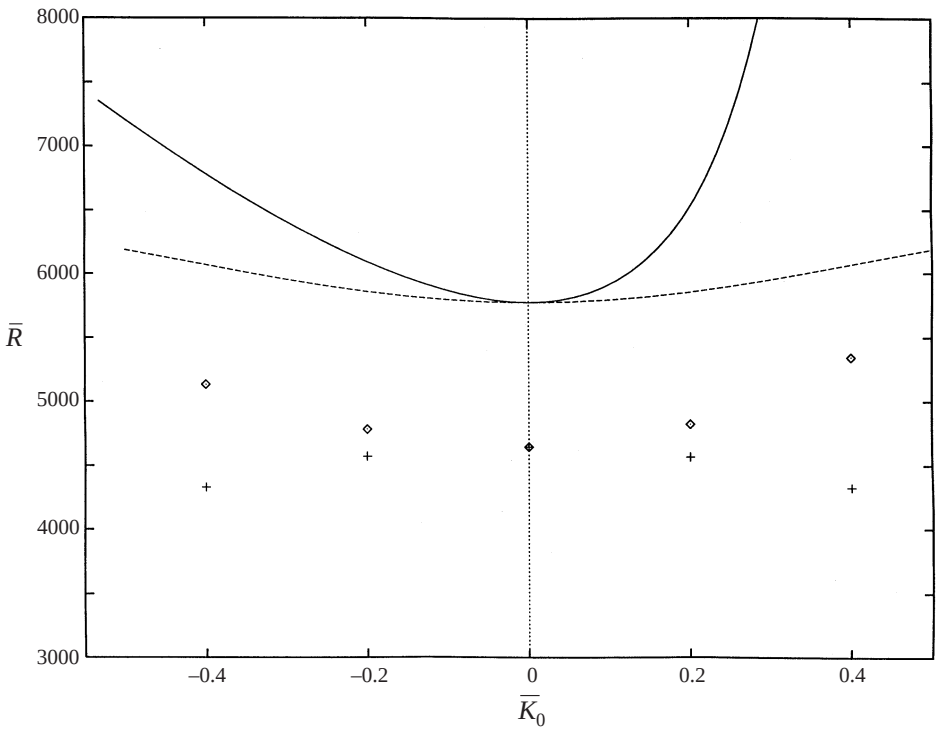

FIGURE 12. $\overline{R_c}$ plotted against $\overline{K_0}$ for $\mu(T) = 1 - K_2 T$ (—) and $\mu(T) = \mathrm{e}^{-K_1 T}$ (- - -) together with values of $\overline{R_c^{NL}}$ for $\mu(T) = 1 - K_2 T$ ($\diamond$) and $\mu(T) = \mathrm{e}^{-K_1 T}$ (+).

much lower than R_c, as was found in the experiments of Davies & White (1928) for example. In this situation there appears to be a bypass mechanism as described by Morkovin (1969). The present results would suggest that the same mechanism may occur for flows with temperature-dependent viscosity and so the qualitative differences in R_c between the viscosity models may not occur in noisy practical applications. In figure 12 we plot $\overline{R_c^{NL}}$, a nonlinear critical Reynolds number based on average viscosity defined in § 2, against $\overline{K}_0$. Interestingly, with the removal of the bulk effect it is clear that the secondary flows corresponding to viscosity model 2 are more stable than those corresponding to viscosity model 1. This is in the sense that $\overline{R_c^{NL}} > \overline{R_c^{NL}}^0$ for the former model, where $\overline{R_c^{NL}}^0$ represents the isothermal nonlinear critical Reynolds number based on average viscosity, whereas $\overline{R_c^{NL}} < \overline{R_c^{NL}}^0$ for the secondary flows whose viscosity is given by the latter model. We found that none of the flows considered here was stable to all Floquet parameter pairs, (d, b), and so they would not be expected to exist in equilibrium in practice. The order of magnitude of growth rates of three-dimensional disturbances would suggest that the thermal flows lose stability to a rapid growth of a three-dimensional secondary disturbance in a similar manner to the isothermal flows.

Appendix. Nonlinear primary bifurcation terms

$$\begin{aligned} \boldsymbol{k}\cdot\nabla\times\breve{\boldsymbol{u}}\cdot\nabla\breve{\boldsymbol{u}} = {} & -\Delta_2\psi\Delta_2\phi_z + \Delta_2\phi_y(\phi_{xzz}+\psi_{yz}) - \Delta_2\phi_x(\phi_{yzz}-\psi_{xz}) \\ & -\Delta_2\psi_x(\phi_{xz}+\psi_y) - (\phi_{yz}-\psi_x)\Delta_2\psi_y + \Delta_2\phi\Delta_2\psi_z, \end{aligned} \tag{A 1}$$

$$\begin{aligned}\boldsymbol{k}\cdot\nabla\times(\nabla\times\breve{\boldsymbol{u}}\cdot\nabla\breve{\boldsymbol{u}}) &= (\nabla^2\phi_x+\psi_{yz})\left(\psi_{xxy}-\phi_{yyxz}\right)-(\nabla^2\phi_y-\psi_{xz})\left(\phi_{xxyz}+\psi_{xyy}\right)\\ &+(\nabla^2\phi_{xx}+\psi_{xyz})\left(2\left[\phi_{xxz}+\psi_{xy}\right]-\Delta_2\phi_z\right)-(\nabla^2\phi_{yy}-\psi_{xyz})\left(2\left[\psi_{xy}-\phi_{yyz}\right]+\Delta_2\phi_z\right)\\ &+2\left[\phi_{xyz}(\psi_{yyz}-\psi_{xxz})-\psi_{xx}\psi_{yyz}-\psi_{yy}\psi_{xxz}+(\phi_{xyzz}+\Delta_2\phi_{xy})(\psi_{yy}-\psi_{xx}+2\phi_{xyz})\right]\\ &+\Delta_2\phi_y(\phi_{xxyz}-\psi_{xxx})+(\phi_{xxyz}+\psi_{yyx})(\phi_{yzz}-\psi_{xz})+\Delta_2\phi_x(\phi_{xyyz}+\psi_{yyy})\\ &+(\phi_{xyyz}-\psi_{xxy})(\phi_{xzz}+\psi_{yz})+\nabla^2\Delta_2\phi_x(\phi_{xz}+\psi_y)+\nabla^2\Delta_2\phi_y(\phi_{yz}-\psi_x)\\ &-\Delta_2\phi\nabla^2\Delta_2\phi_z-\Delta_2\phi_x(\nabla^2\phi_{xz}+\psi_{yzz})+\Delta_2\phi_y(\psi_{xzz}-\nabla^2\phi_{yz}).\end{aligned}\tag{A 2}$$

REFERENCES

Bayly, B. J., Orszag, S. A. & Herbert, T. 1988 Instability mechanisms in shear-flow transition. *Ann. Rev. Fluid Mech.* **20**, 359–391.

Davies, S. J. & White, C. M. 1928 An experimental study of the flow of water pipes of rectangular section. *Proc. R. Soc. Lond.* A **119**, 92–107.

Ehrenstein, U. & Koch, W. 1989 Nonlinear bifurcation study of plane Poiseuille flow. *DLR Res. Rep.* FB 89–42.

Ehrenstein, U. & Koch, W. 1991 Three-dimensional wavelike equilibrium states in plane Poiseuille flow. *J. Fluid Mech.* **228**, 111–148.

Elofsson, P. A. & Alfredsson, P. H. 1998 An experimental study of oblique transition in plane Poiseuille flow. *J. Fluid Mech.* **358**, 177–202.

Grohne, D. 1969 Die Stabilität der ebenen Kanalströmung gegenüber dreidimensionalen Strörungen von endlicher Amplitude. *AVA Göttingen, Rep.* 69 A 30.

Herbert, T. 1981 A secondary instability mechanism in plane Poiseuille flow. *Bull. Am. Phys. Soc.* **26**, 1257.

Herbert, T. 1983 On perturbation methods in nonlinear stability theory. *J. Fluid Mech.* **126**, 167–186.

Klebanoff, P. S., Tidstrom, K. D. & Sargent, L. M. 1962 The three-dimensional nature of boundary-layer instability. *J. Fluid Mech.* **12**, 1–34.

Kozlov, V. V. & Ramazanov, M. P. 1984 Development of finite-amplitude disturbances in Poiseuille flow. *J. Fluid Mech.* **147**, 149–157.

Meksyn, D. 1964 Stability of laminar flow between parallel planes for two- and three-dimensional finite disturbances. *Z. Physik* **178**, 159–172.

Meksyn, D. & Stuart, J. T. 1951 Stability of viscous motion between parallel planes for finite disturbances. *Proc. Soc. Lond.* A **208**, 517–526.

Morkovin, M. V. 1969 On the many faces of transition. In *Viscous Drag Reduction.* (ed. C. S. Wells), pp. 1–31. Plenum.

Nishioka, M., Iida, S. & Ichikawa, Y. 1975 An experimental investigation of the stability of plane Poiseuille flow. *J. Fluid Mech.* **72**, 731–751.

Nishioka, M., Iida, S. & Kanbayashi, S. 1978 An experimental investigation on the subcritical instability in plane Poiseuille flow. In *Proc. 10th Turbulence Symp., Inst. Space Aeron. Sci., Tokyo University,* pp. 55–62 (in Japanese).

Orszag, S. A. 1971 Accurate solution of the Orr-Sommerfeld stability equation. *J. Fluid Mech.* **50**, 689–703.

Orszag, S. A. & Kells, L. C. 1980 Transition to turbulence in plane Poiseuille and plane Couette flow. *J. Fluid Mech.* **96**, 159–205.

Orszag, S. A. & Patera, A. T. 1980 Subcritical transition to turbulence in plane parallel flows. *Phys. Rev. Lett.* **45**, 989–993.

Orszag, S. A. & Patera, A. T. 1983 Secondary instability of wall bounded shear flows. *J. Fluid Mech.* **128**, 347–385.

Pekeris, C. L. & Shkoller, B. 1969 The neutral curves for periodic perturbations of finite amplitude of plane Poisuille flow. *J. Fluid Mech.* **39**, 629–639.

Potter, M. C. & Graber, E. 1972 Stability of plane Poiseuille flow with heat transfer. *Phys. Fluids* **15**, 387–391.

Potter, M. C. & Smith, M. C. 1968 Stability of an unsymmetrical plane flow. *Phys. Fluids* **11**, 2763–2764.

Pugh, J. D. & Saffman, P. G. 1988 Two-dimensional superharmonic stability of finite amplitude waves in plane Poiseuille flow. *J. Fluid Mech.* **194**, 295–307.

Rozhdestvensky, B. L. & Simakin, I. N. 1984 Secondary flows in a plane channel: their relationship and comparison with turbulent flows. *J. Fluid Mech.* **147**, 261–289.

Schäfer, P. & Herwig, H. 1993 Stability of plane Poiseuille flow with temperature dependent viscosity. *Intl J. Heat Mass Transfer* **36**, 2441–2448.

Stuart, J. T. 1960 On the non-linear mechanics of wave disturbances in stable and unstable parallel flows. *J. Fluid Mech.* **9**, 353–370.

Wall, D. P. 1996 Thermal effects in fluid flow. PhD thesis, University of Strathclyde, Glasgow, UK.

Wall, D. P. & Wilson, S. K. 1996 The linear stability of channel flow of fluid with temperature-dependent viscosity. *J. Fluid Mech.* **323**, 107–132.

Watson, J. 1960 On the non-linear mechanics of wave disturbances in stable and unstable parallel flows. Part 2. The development of a solution for plane Poiseuille flow and for plane Couette flow. *J. Fluid Mech.* **9**, 371–389.